Hydrology Research 57 (2026) 100005

Contents lists available at ScienceDirect

Hydrology Research

journal homepage: www.elsevier.com/locate/issn/1998-9563

Synthesizing flood exposure maps for comprehensive risk assessment

Eden Seifu Gebre[a,*], Alemseged Tamiru Haile[b], Tilaye Worku Bekele[c], Wegayehu Asfaw[c,d], Mark A. Trigg[e]

[a] Africa Centre of Excellence for Water Management (ACEWM), Addis Ababa University, Addis Ababa, Ethiopia
[b] International Water Management Institute (IWMI), P. O. Box 5689, Addis Ababa, Ethiopia
[c] Faculty of Hydraulic and Water Resources Engineering, Institute of Water Technology, Arba Minch, University, P. O. Box 21, Arba Minch, Ethiopia
[d] Department of Water Resources, Faculty of Geo-Information Science and Earth Observation (ITC), University of Twente, 7522 NH Enschede, the Netherlands
[e] School of Civil Engineering, University of Leeds, Leeds, United Kingdom

ARTICLE INFO

Keywords:
Flood exposure mapping
SAR-derived flood maps
Citizen Science
Urban flood
Addis Ababa

ABSTRACT

Flooding poses a major risk to rapidly growing cities like Addis Ababa, Ethiopia, where urban expansion, increasing impervious surfaces, and climate change continually intensify flood hazards. This study evaluates urban flood exposure by systematically comparing flood maps derived from fundamentally distinct methodologies. The primary objectives are to (i) delineate empirical flood exposure by integrating a multi-temporal Sentinel-1 SAR inundation map (2017–2023) with datasets on population, buildings, and road networks; and (ii) assess spatial agreement among exposure maps produced via hydrodynamic modeling, machine learning-based susceptibility analysis, and SAR mapping. The SAR-derived map was validated using a synthesized dataset of institutional records and citizen-science observations. Results reveal that 57 km^2 of buildings and 18 km of road networks are highly exposed to recurrent flooding. Furthermore, a critical spatial comparison using Jaccard (0.014–0.072) and Dice (0.027–0.143) coefficients, Moran's I, and topographic correlation analysis revealed profound disagreement in flood risk extent and spatial distribution. These extreme discrepancies mathematically confirm the models capture distinct physical mechanisms rather than acting as redundant proxies. Consequently, relying on a single mapping framework inevitably biases urban flood risk estimation. This study provides baseline evidence advocating for a multi-criteria approach to support robust urban disaster risk management.

1. Introduction

Flooding is among the most devastating natural disasters. According to the International Emergency Events Database (EM-DAT), flood-related disasters killed over 7 million people globally between 1900 and 2022, and the resulting socioeconomic losses were nearly USD 9.6 trillion (CRED, 2022). In Africa, particularly Sub-Saharan Africa, flooding is a recurrent and growing challenge, with

* Corresponding author.
E-mail address: eden.seifu@aau.edu.et (E.S. Gebre).

https://doi.org/10.1016/j.hydrch.2026.100005
Received 18 February 2026; Received in revised form 11 April 2026; Accepted 3 May 2026
Available online 2 June 2026
1998-9563/© 2026 The Author(s). Published by Elsevier Ltd on behalf of Italian Hydrological Society (IHS). This is an open access article under the CC BY-NC-ND license (http://creativecommons.org/licenses/by-nc-nd/4.0/).

recent events leading to widespread displacement and infrastructure damage across multiple countries (Baddianaah, 2023; Ramiaramanana & Teller, 2021; UN OCHA, 2024). Urban areas are especially vulnerable due to rapid population growth, unplanned expansion, and increasing pressure on drainage systems.

Addis Ababa, the capital city of Ethiopia, reflects many of these challenges. The city experiences both fluvial and pluvial flooding, driven by intense seasonal rainfall, rapid urban expansion, and inadequate drainage infrastructure (Birhanu et al., 2016; Moges et al., 2014). In recent years, the expansion of impervious area has significantly altered the natural hydrological response of the city, increased surface runoff and reducing infiltration capacity (Moisa et al., 2022). These factors, combined with projected increases in extreme rainfall linked to climate change, are expected to further intensify urban flood hazards in the city.

Flood maps are essential tools for understanding and managing flood risk, informing decisions in emergency response, infrastructure planning, and long-term risk reduction. They can be broadly classified into maps of observed flooding and maps of potential flooding. Observed flood maps, often derived from remote sensing (e.g., synthetic aperture radar imagery) (Lin et al., 2016; Feizbahr et al., 2025), provide direct evidence of past flood events. In contrast, potential flood maps are generated through modeling approaches and can be further divided into hydrodynamic flood hazard maps and flood susceptibility maps. Hydrodynamic models simulate flood processes under specific scenarios to estimate flood extent, depth, and velocity (Mani et al., 2013; Abdelkarim et al., 2019). Flood susceptibility maps, on the other hand, identify areas prone to flooding based on environmental factors using statistical or machine learning techniques (Feizbahr et al., 2025; Montien Tique et al., 2026). Each type of map offers distinct advantages but also carries inherent limitations. Satellite-based mapping may miss short-lived flood events or suffer from acquisition timing and image quality issues; hydrodynamic model outputs are highly sensitive to input data quality and parameter choices; and susceptibility maps are influenced by the selection of conditioning factors and the specific modeling strategy employed (De Moel et al., 2009; De Brito & Evers, 2016; Bentivoglio et al., 2022).

As a result of these differences in data sources, assumptions, and modeling frameworks, flood maps generated from different approaches often show inconsistent representations of flood extent. Previous studies have reported inconsistencies between remotely sensed flood maps and hydrodynamic model outputs, as well as among different modeling approaches (Bekele et al., 2022). Since flood exposure assessments are directly derived from these flood maps, such discrepancies can significantly influence the estimation of exposed population, infrastructure, and assets. However, limited studies have systematically examined how these differences propagate into flood exposure assessments, particularly in urban environments.

In data-scarce environments, the challenge is further compounded by the limited availability of reliable ground-based flood observations for validation. Citizen science has emerged as a powerful approach specifically for flood mapping and flood map validation. Recent studies have demonstrated that citizen-generated data can directly support flood mapping and validate remotely sensed flood products (Sejinja et al., 2025). Participatory flood mapping in African cities has produced validated flood hazard maps (Tiepolo et al., 2025), while social media and mobile app reports have been used to map real-time inundation and validate model outputs (Sejinja et al., 2025). These examples confirm that citizen science can effectively complement remote sensing and hydrodynamic models for flood mapping and validation, provided that spatial coverage and reporting protocols are carefully designed.

The present study builds on this foundation by integrating a social-media-based citizen-science campaign with multi-temporal Sentinel−1 SAR mapping and institutional data to validate observed flood extents and identify exposure hotspots in Addis Ababa. It tests the hypothesis that flood-exposure estimates differ depending on whether they are derived from observed flood maps, hydrodynamic model outputs, or machine-learning-based susceptibility maps. Using Addis Ababa as a case study, the research provides a systematic comparison of the contextual strengths and limitations of each approach for urban flood-exposure assessment. Specifically, the study (1) identifies and maps flood-exposed areas using flood maps derived from multi-temporal Sentinel−1 SAR imagery validated with citizen-science observations and institutional data, and (2) evaluates the spatial agreement and discrepancies among flood-exposure maps generated from SAR observations, hydrodynamic modelling, and machine-learning techniques. By comparing multiple methodological pathways, this work clarifies how exposure estimates vary across mapping methods in urban environments and demonstrates the added value of combining observed and modelled information for more robust flood-risk assessment.

2. Material and methods

2.1. Study area

Addis Ababa is Ethiopia's capital, located in the geographic center of the country with administration divided into eleven sub-cities. It is the largest city in the country and plays a central political, economic, and symbolic role in Ethiopia with a total projected population of over 4 million people in 2025 (CSA, 2013). All the sub-cities in the inner city have high population density compared to sub-cities found in peripheral areas. However, based on the city's development plan (2017–2027), the undertaken works of inner-city renewal, corridor redevelopment, land expropriation, and expansion to low-density areas appear to be influencing a shift in density distribution from the inner city towards the periphery. There is a fast rate of urban expansion resulting in more built-up areas in the city.

Addis Ababa is located in the central highlands of Ethiopia geographically between 8°50′N to 9°5′N and 38°38′E to 38°54′E covering a surface area of about 527 km^2 (Fig. 1a). The altitude range extends from the highest peak at Mount Entoto at 3027 m to 2033 m in the lower part of Akaki plain with average elevation of 2517 m. The city's undulating terrain, with mountains, slopes, plateaus, and plains, along with deeply incised rivers, significantly contributes to flooding. Addis Ababa experiences a unimodal rainfall pattern with three distinct seasons (Asfaw et al., 2023): the short rainy season (Belg) from February to May, the main rainy season (Kiremt) from June to September, and the dry season (Bega) lasting from October to December, extending into January of the

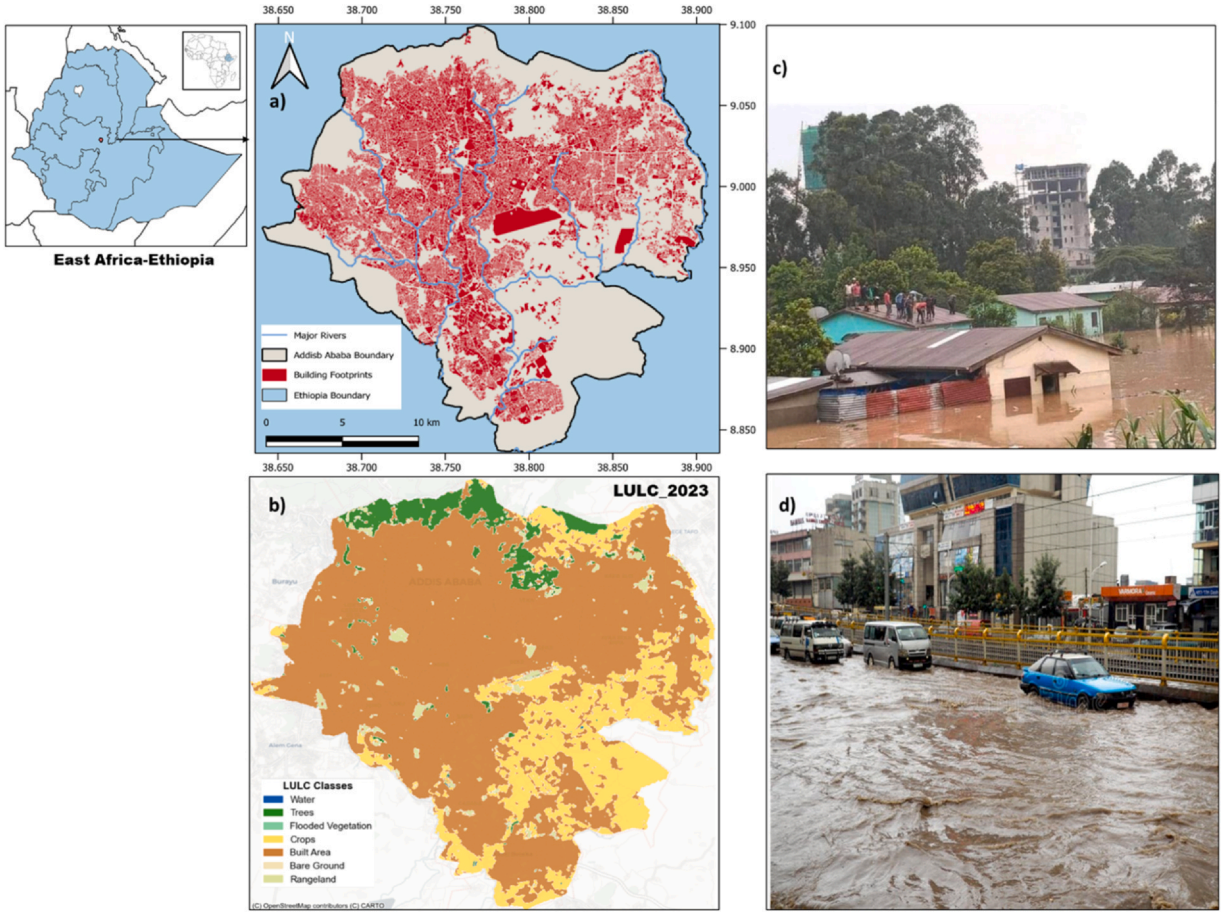


Fig. 1. Overview of the and local flood impacts. (a) Addis Ababa city boundary and spatial distribution of building footprints. (b) Sentinel − 2 Land Use/Land Cover (LULC) map at 10-m resolution (data: Esri, 2023). (c) Damage to residential property, showing firefighters inspecting flooded homes on August 18, 2021 (Photo: Amanuel Sileshi / AFP). (d) Transport infrastructure disruption, with vehicles navigating flooded urban roads on July 21, 2019 (Photo: Tim Wege / Depositphotos).

following year. The average annual rainfall for Addis Ababa is 1184 mm. The city is rich with major rivers: Kebena, Bulbula, Little Akaki and Big Akaki rivers and numerous small streams. However, these water bodies present a significant risk to.

the city due to frequent fluvial flooding events. This risk is exacerbated by alterations in river morphology, primarily resulting from sedimentation, which diminishes their conveyance capacity. Furthermore, the expansion upon riverbanks, with settlements extending into and beyond designated buffer zones, further contributes to the heightened exposure of the city to flooding.

The city's land use/land cover (LULC) is majorly characterized by urban infrastructure (Fig. 1b). Due to rapid urbanization, built-up areas now cover roughly 327.57 km^2 over 70% of the total study area leaving the remaining natural and agricultural land classes as minor fractions of the landscape (Esri, 2023). This growing footprint of impervious surfaces, paired with inadequate drainage and poor land management, drives frequent flooding that heavily disrupts residents and transportation networks. Recent notable events include the severe flash flooding of 17 August 2021 that killed at least seven people and inundated several neighborhoods after torrential rains (FloodList, 2021; Al Jazeera, 2021) and the prolonged inundation during the earlier-than-usual second rainy season of April–May 2023 that caused widespread flood disruption across the city (ReliefWeb, 2023; Ethiopian Meteorology Institute, 2023).

2.2. Flood exposure maps

The methodology for this study consists of two main steps. The initial step is to identify and map the city's flood exposure using remotely sensed flood inundation maps with exposure indicators. This map will be referred to as the SAR flood exposure map throughout the paper, since it's derived from a multi-temporal Sentinel − 1 Synthetic Aperture Radar (SAR) dataset. The second step involves a comparative analysis of flood exposure across different maps developed for the city using various methods, including the SAR flood exposure map generated in the first step. These maps are (i) a flood exposure map developed by intersecting the 1-in − 100-year flood extent map, produced using hydrodynamic flood modeling, with the Google Open Buildings Dataset Version 1 to identify exposed buildings by Carr et al. (2024), referred to as the modeled flood exposure map throughout the paper, and (ii) a flood susceptibility map, which was produced by using machine learning techniques using input datasets including hydro meteorological, social, and environmental parameters by Asfaw et al. (2025).

Table 1
Summary of datasets used for SAR flood exposure map development.

Data	Description	Form-at	Source
Population density	High-resolution (30 m) population density maps produced from a combination of buildings and population estimates	Geotiff	Humanitarian Data Exchange(HDE) dataset https://hdl.handle.net/10986/33700
Building footprint	OpenStreetMap(OSM) building footprint data refined with supplementary building footprint data from Ethiopian Geospatial Information Agency	Vector	https://www.openstreetmap.org/copyright/en Ethiopian Geospatial Information Agency
Major road network	OpenStreetMap Road Network Attributes.	Vector	https://www.openstreetmap.org/copyright/en
SAR flood map	10 m flood inundation areas processed and aggregated for the duration of 2017–2023 from S − 1 SAR dataset	Geotiff	Modified fromBekele et al. (2022)
Flood observations	Citizen scientists geo-tagged flood pictures and videos and surveyed flood observations	CSV	Citizen science based flood detection Addis Ababa city fire and disaster risk management commission (AAFDRMC). (2021) *Assessment and Profiling of Flood Disaster Risk of Addis Ababa City*

2.2.1. SAR flood exposure map development

The flood inundation map used in this study is adopted and modified from the flood mapping algorithm developed by Bekele et al. (2022) using a multi-temporal Sentinel − 1 SAR dataset. In Bekele et al. (2022), the flood inundation maps were generated from April to November of 2017–2020 (4 years) by using the Root of Normalized Image Difference change detection method and VH polarization of the SAR dataset, which resulted in an overall accuracy of 95% and a kappa of 0.86 when compared against ground truth data. For this study, the flood inundation maps were generated for 3 additional years, extending the temporal coverage to 7 years (from April to November of 2017–2023) to create overlap with the time frame of the ground-based flood observations.

This study utilizes three key indicators of exposure: population density (Ziegelaar & Kuleshov, 2022), building footprint data, and road network density (Papilloud et al., 2019) to characterize flood exposure within the study area (Table 1). The 30 m population density dataset (Humanitarian Data Exchange) is produced by WorldPop methods that combine building footprints with census microdata and dissymmetric modelling, yielding gridded estimates of people per pixel. This layer is complementary to (but independent of) the building footprint layer because it accounts for varying occupancy rates and household sizes, whereas building footprints represent physical structures only. The building footprint data utilized in this study were primarily sourced from the OpenStreetMap (OSM) database. Recognizing inherent limitations in the completeness of the OSM dataset (Herfort et al., 2023), particularly in settlement areas characterized by sparse building structures within the city, the initial dataset was refined with supplementary data acquired from the Ethiopian Space Science and Geospatial Institute (SSGI).

2.2.1.1. Observed flood data

2.2.1.1.1. Citizen science-based flood detection program. A foundational element of this study was the establishment of a citizen science initiative. A total of over 260 volunteer adult residents, referred to as citizen scientists, were recruited to assist with two primary tasks: establishing an observational dataset for validating the SAR-derived flood map and defining the thresholds for flood hotspots (detailed in Section 2.2.1.2). It is important to note that this same group of > 260 volunteers contributed to both the collection of geo-tagged photos/videos and the household survey. These volunteer members were recruited by approaching them in person, via telephone, or through message conversations. The aim of the work was clearly described, and they were added to the project only after providing their consent. A Telegram public group named “Addis Ababa Flood Pictures” was created to coordinate data collection. Added members were encouraged to invite other citizen scientists to the group using invite links, which were also shared on other public Telegram groups to achieve wider spatial representation across the city.

The citizen scientists collected the flood data from April to September 2023, which aligns with the main rainy season of the study area. Importantly, the 2023 wet season commenced earlier than typical, with heavy rainfall events occurring in April, resulting in widespread flood inundation throughout the city. This unusual rainfall pattern provided a unique opportunity to observe flood events and gather valuable in-situ data.

For taking geo-tagged pictures and videos, citizen scientists used a tool called “GPS Map Camera Lite”. It is an easy-to-use mobile camera application, available on the Play Store, which stamps GPS coordinates, date and time, and altitude details on photos and videos when captured. Although smartphone GPS accuracy in urban environments is typically ± 5–10 m, this approach is adopted in citizen-science flood studies (Tran et al., 2024 and references therein). For contributions with missing attributes (e.g., GPS location or date and time) or having blurred pictures or videos, an immediate feedback request is given to include the missing items or to possibly improve the quality by taking pictures from a higher standpoint with a recognizable reference. In some cases, if they were not able to capture a picture or video of a flood event due to circumstances, they only share the information with the group through text using a clear broad description of the area using the street name or any other well-known reference, including the date and the approximate time of the event.

To ensure the quality and relevance of the information reported from citizen scientists, exceptions such as flood pictures or videos with a time or location tag that does not overlap with the study area and study period were primarily excluded. To address the inherent positional limitations of mobile GPS and ensure reliability, we performed field verification of a subset of the reported locations to further check the validity of geographic coordinates and gather additional contextual information. A total of 102 point-based flood observations were obtained from the citizen scientists, with 77 deemed suitable for analysis after the data quality assessment.

2.2.1.1.2. Institutional data. The other set of validation data employed to assess the performance of the SAR-derived flood map was sourced from the Addis Ababa City Fire and Disaster Risk Management Commission (AAFDRMC). To map and profile flood risk spots across the city, the commission conducted a comprehensive city-scale assessment based on extensive field observations collected up to 2021 (AAFDRMC, 2021). 342 geo-referenced hazard spots were identified in the city. This assessment categorized flood risk across sub-cities into five classes ranging from very low to very high based on the frequency of flood incidents, density of population, poor infrastructure, and socio-economic conditions. For the validation process, only the 168 locations classified as very high risk (50 spots) and high risk (118 spots) were utilized. This selection aligns with the study's overall objective of evaluating consensus specifically on high flood exposure zones across all three mapping methods.

2.2.1.2. Defining thresholds for flood hotspots. Flood hotspots (e.g., Jalayer et al., 2014) are areas potentially experiencing high casualties and damage, as such, necessitate immediate or long-term mitigation actions. In this study, for the designation of flood hotspots, a systematic set of criteria was employed, specifically tailored to the characteristics of flooding observed. Surveys utilizing questionnaires were employed to collect information from the public regarding factors such as the frequency of flooding and the size of the population impacted to designate a certain location as a flood hotspot. The survey involved 60 adult participants who were randomly selected from the aforementioned pool of $>$ 260 citizen scientists, ensuring broad spatial coverage and leveraging their observational experience. In addition to the survey responses, the threshold of a minimum of ten households affected at least twice per year was also informed by the authors' expert knowledge and long-term familiarity with flooding patterns in Addis Ababa. This combined approach (community perception + expert judgement) helps ensure the threshold is both locally relevant and practically meaningful for identifying high-exposure hotspots in the urban context. This methodological approach underscores a critical premise: local insights, knowledge, and experiential data hold significant scientific value, despite their inherent limitations related to spatial patchiness and resolution.

The results of the survey revealed that a community typically perceives a particular area as a flood hotspot when flooding events affect a minimum of ten households at least twice in a year. These threshold values were systematically integrated with layers representing population density and SAR flood inundation maps. Pixels with a resolution of 30 m within the population density layer containing fewer than ten households were excluded, adhering to the survey-defined threshold. To minimize the exclusion of adjacent pixels that collectively exceed the threshold of ten households, a neighborhood analysis was conducted. An aggregate of household counts was calculated for each pixel using a non-overlapping three-by-three-pixel grid. This approach ensures that areas with household counts marginally below the established threshold, yet near areas exceeding the threshold, are duly considered for inclusion in the analysis.

2.2.1.3. Validating SAR flood map with observed flood data. Validating continuous remote sensing products using discrete in-situ observations inherently presents temporal and spatial challenges, particularly in data-scarce urban environments. To robustly validate the SAR-derived flood map, which represents cumulative inundation over the 2017–2023 rainy seasons, we employed a dual-source point-to-pixel validation approach.

Temporally, the validation data brackets the SAR composite period. The AAFDRMC dataset provides a verified historical baseline of persistent flood hotspots identified up to 2021. Conversely, the citizen-science dataset provides high-confidence observations from the severe April-September 2023 rainy season. Because urban flooding in Addis Ababa is largely driven by static topographic and infrastructural factors, hotspots are generally persistent across years. Therefore, combining these datasets effectively captures the flooding spanning the 2017–2023 SAR temporal window.

Spatially, we acknowledge that citizen-science observations are opportunistic and do not offer 100% continuous coverage, which introduces a sampling bias toward populated or accessible areas. However, this aligns with the study's primary objective of assessing high-exposure urban zones. To establish a clear 'validity-area' for statistical assessment, the validated point data (from both citizen science and AAFDRMC) were rasterized to match the exact 10 m resolution of the SAR grid. A binary confusion-matrix analysis was then performed. Rather than evaluating the entire continuous map, this analysis specifically tests the SAR model's True Positive Rate (its ability to accurately detect known, ground-verified flooded pixels), demonstrating its reliability in mapping critical urban hotspots despite the lack of spatially continuous ground-truth data.

We used accuracy measures such as overall accuracy, F1-score, Cohen's kappa coefficient (Cohen, 1960), and Matthews correlation coefficient (MCC) (Matthews, 1975), which are depicted in Table 2. F1-score measures the harmonic mean of the precision and recall, where precision represents the fraction of correctly identified flooded pixels to the total number of as flooded by the SAR map, while recall is the fraction of the observed flooded pixels that are correctly identified as flooded in the SAR flood map. The F1 score ranges from 0 to 1, where a higher F1 score indicates better balance between precision and recall. Similarly, the Kappa coefficient measures statistical agreement between observed agreement (Po) and expected agreement (Pe), and a value higher than 0.80 indicates strong agreement; values between 0.40 and 0.80 show moderate agreements, and coefficients below 0.40 represent weak agreement (Landis & Koch, 1977). Furthermore, Matthews Correlation Coefficient (MCC) values close to 1 represent perfect agreement, the value of 0 is interpreted as random prediction, and the value of -1 is interpreted as complete opposite.

2.2.1.4. Spatial intersection. To generate the SAR flood exposure map, the SAR-derived flood inundation map (where thresholds of flood hotspots were applied) was overlaid and intersected with exposure indicator layers (population, buildings, and roads) after resampling to bring every layer to a similar resolution. To reduce radar shadow and layover effects caused by buildings on SAR flood maps (Rahman & Thakur, 2018), buffer zones were applied around the building footprint. We tested a range of buffer sizes (e.g., 10 m, 20 m, and 50 m) and inspected how the results change to determine the most suitable size around the buildings. A buffer zone of 10 m was implemented.

Table 2
Formulas related to accuracy assessment SAR derived flood map.

Metrics	Formula
Overall accuracy	$\frac{TP+TN}{TP+TN+FP+FN}$
F1-Score	$2*\left(\frac{Precision*Recall}{Precision+Recall}\right)$
Cohen's Kappa Coefficient	$\frac{p_o-p_e}{1-p_e}$
Matthews Correlation Coefficient (MCC)	$\frac{TP*TN-FP*FN}{\sqrt{(TP+FP)(TP+FN)(TN+FP)(TN+FN)}}$

2.2.2. Comparative analysis of flood exposure across multiple maps

The second methodological step presents a quantitative analysis of flood exposure among the SAR flood exposure map generated in the first step, the modeled flood exposure map, and the flood susceptibility map, both derived from prior research outputs. By measuring the similarities and differences in flood exposure extent and locations, we aim to highlight the level of agreement and divergence among the maps. These insights can be used to underscore the importance of using multiple maps to achieve a comprehensive understanding of flood risks.

2.2.2.1. Modeled flood exposure map. The modeled flood exposure map was generated by Carr et al. (2024) using a rain-on-grid 2D hydrodynamic model in HEC-RAS 6 (diffusion wave solver). To validate the model, the authors simulated a real minor flood event on 6 September 2017 using ERA5 reanalysis precipitation and achieved good agreement with Sentinel − 2-derived inundation extents (81% hit rate, 73% critical success index). For the primary exposure mapping, the model applied uniform design rainfall events based on local Intensity-Duration-Frequency (IDF) curves derived from in situ rain gauge data for Addis Ababa (De Paola et al., 2018). Using a 24-hour hypothetical storm profile, they simulated synthetic 1-in − 5-year and 1-in − 100-year return period events. Finally, the resulting flood extents were intersected with the Google Open Buildings Dataset (Version 1) to identify exposed structures, which were then converted into a 100 m resolution exposure raster.

For the present study, only the flood exposure raster map generated for the extreme 1-in − 100-year flood event was utilized. The map exhibits a range of exposure levels, spanning from 0 to 561 buildings per pixel, corresponding to areas from no flood exposure to very high flood exposure, respectively. However, to maintain consistency with the methodology employed in the generation of the SAR flood exposure defining thresholds for hotspots, we set a threshold (above 263 buildings per 100 m pixel) based on our knowledge of the study area, designed to identify pixels exhibiting very high flood exposure.

2.2.2.2. Flood susceptibility map. The flood susceptibility map by Asfaw et al. (2025) was developed by conducting an in-depth analysis of twenty-eight flood conditioning factors derived from open-access earth observation datasets to develop flood susceptibility prediction models of Addis Ababa and the surrounding Akaki catchment. Using a systematic approach, they identified relevant flood conditioning factors and applied a random forest-based machine learning model to integrate these factors and assess flood susceptibility in the study area. The map delineates susceptibility classes on a scale of 0–5, where 0 signifies an insusceptible condition and 5 denotes a very high susceptibility to flooding. Consistent with the methodology taken in generating the SAR flood exposure map of defining thresholds for hotspots, our study similarly prioritized very high and high flood-susceptible pixels while deliberately excluding lower susceptibility classes.

2.3. Spatial patterns and agreement among multiple maps

The SAR flood exposure map generated, the modeled flood exposure map, and the flood susceptibility map collected from the aforementioned sources were subsequently processed to ensure they had the same spatial resolution, extent, and alignment for valid comparison and quantitative geospatial analysis. Notably, the resolution of the SAR flood exposure map is 10 m, a specification that arises from the Sentinel − 1 dataset. In contrast, the modeled flood exposure map is characterized by a resolution of 100 m, while the flood susceptibility map is at a resolution of 30 m. To facilitate the consequent analysis, both the SAR and modeled flood exposure maps were resampled to conform to the 30-meter resolution of the susceptibility map.

The spatial pattern of flooded areas in the individual maps was assessed using Moran's I index (Moran, 1950). It is a measure of spatial autocorrelation, the degree to which flooded pixels and non-flooded pixels are spatially clustered, dispersed, or randomly distributed. The index ranges from − 1 to 1. A positive value indicates clustering of flooded areas, while a negative result indicates a spatial pattern of dissimilarity. The spatial relationship among the flooded areas in each map with their topographic characteristics was also assessed. For this, using a 10 m digital elevation model (DEM) of the study area, obtained from the Ethiopia Space Science and Geospatial Information Institute (SSGI) and resampled to 30 m, topographic variables such as elevation, slope, and distance to the river were generated and classified into five subclasses as presented below in Fig. 2. Distance to river was computed to the nearest stream segment using stream order 2 and higher only (i.e., small headwater tributaries of order 1 were excluded). This choice avoids an artificially high drainage density while still minimizing under representation of channels that contribute to flooding in the urban setting of Addis Ababa. These key topographic variables were used to understand and determine the significance of specific subclasses in relation to flood occurrences across the three distinct maps.

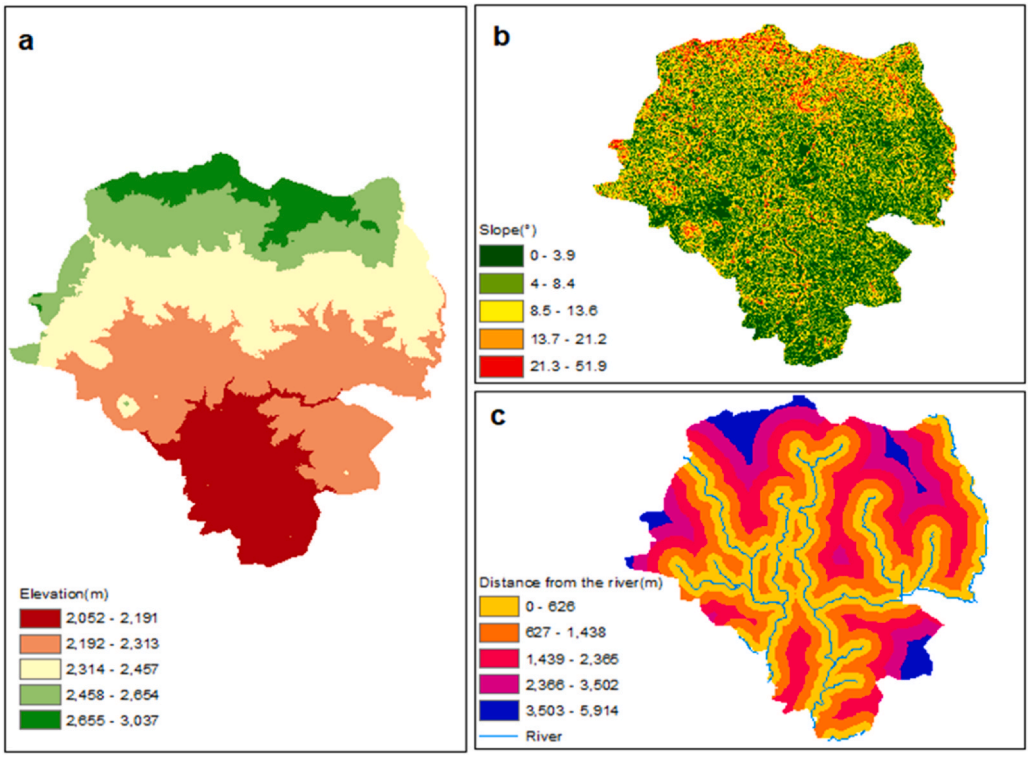


Fig. 2. Topographic variables used in this study are: (a) elevation, (b) slope in degrees (°) and (c) distance from river.

In addition, we systematically assessed the overall agreement between the maps, taking spatial proximity into account (i.e., not just whether flooded pixels match exactly but also how far apart the agreements and disagreements between flooded pixels are). The evaluation encompassed comparisons among three distinct pairs of maps: SAR versus modeled map, SAR versus susceptibility maps, and modeled versus susceptibility maps. To quantify the degree of agreement and the spatial relationships within each pair, we employed the metrics detailed in Table 3.

3. Results

3.1. SAR flood exposure map

This study was able to identify the locations and spatial extents of the flood-exposed buildings and roads of Addis Ababa (see Fig. 3). Flooded locations from SAR-derived flood maps appeared scattered throughout the city, with a notable concentration in low-lying areas. The total inundated area of buildings and length of road exposed was determined to be 57 square km and 18 km,

Table 3
Spatial comparison metrics.

Metrics	Definition	Formula
Jaccard Coefficient (Jaccard,1901)	Measure of overall agreement between two datasets by quantifying the proportion of overlapping areas relative to their union area	$J = \frac{\lvert A \cap B \rvert}{\lvert A \cup B \rvert}$ Where • A and B are the sets of flooded pixels in the two maps • J ranges from 0 (no overlap) to 1 (perfect overlap).
Dice Coefficient (Sørensen,1948)	Measure of similarity between two datasets with emphasis on the intersection	$D = \frac{2 \lvert A \cap B \rvert}{\lvert A \rvert + \lvert B \rvert}$ Where • A and B are the sets of flooded pixels in the two maps • D ranges from 0((no overlap)) to 1(perfect overlap).
Hausdorff Distance (HD) (Hausdorff,1914)	Calculates the maximum distance between two sets of points in a spatial domain	$d_H(A, B) = \max(\sup a \in A \inf b \in B\, d(a, b), \sup b \in B \inf a \in A\, d(a, b))$ Where • A and B are the sets of flooded pixels in the two maps. • d(a,b) is the Euclidean distance between pixel a in set A and pixel b in set B

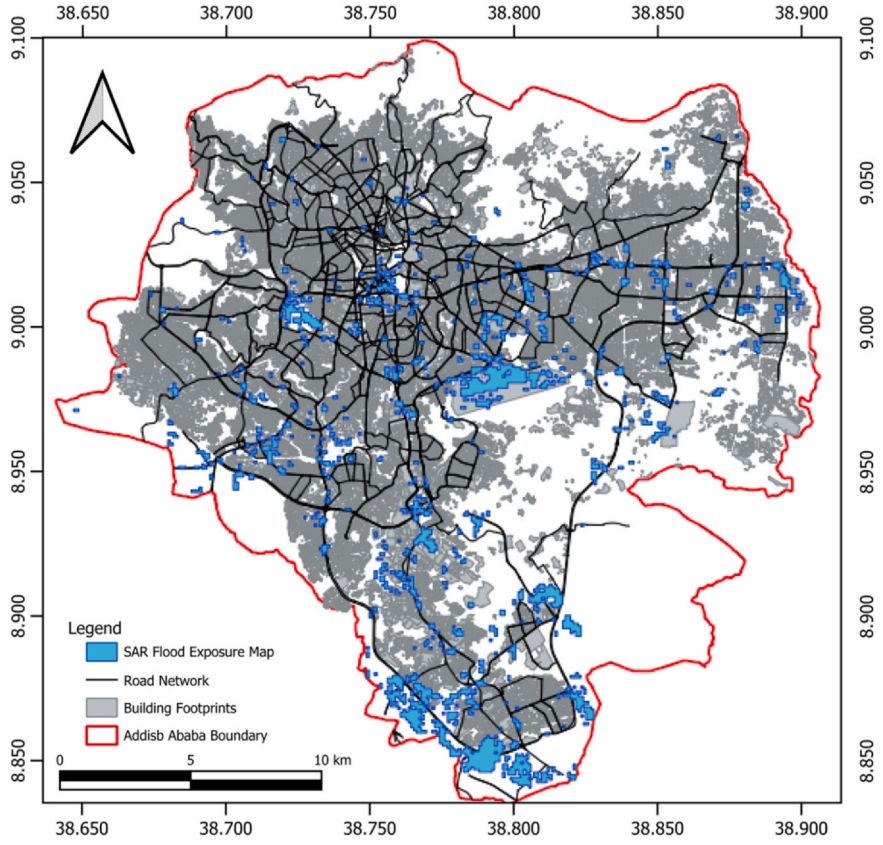


Fig. 3. SAR flood exposure map, highlighting the food inundation extent across the city from 2017 − 2023.

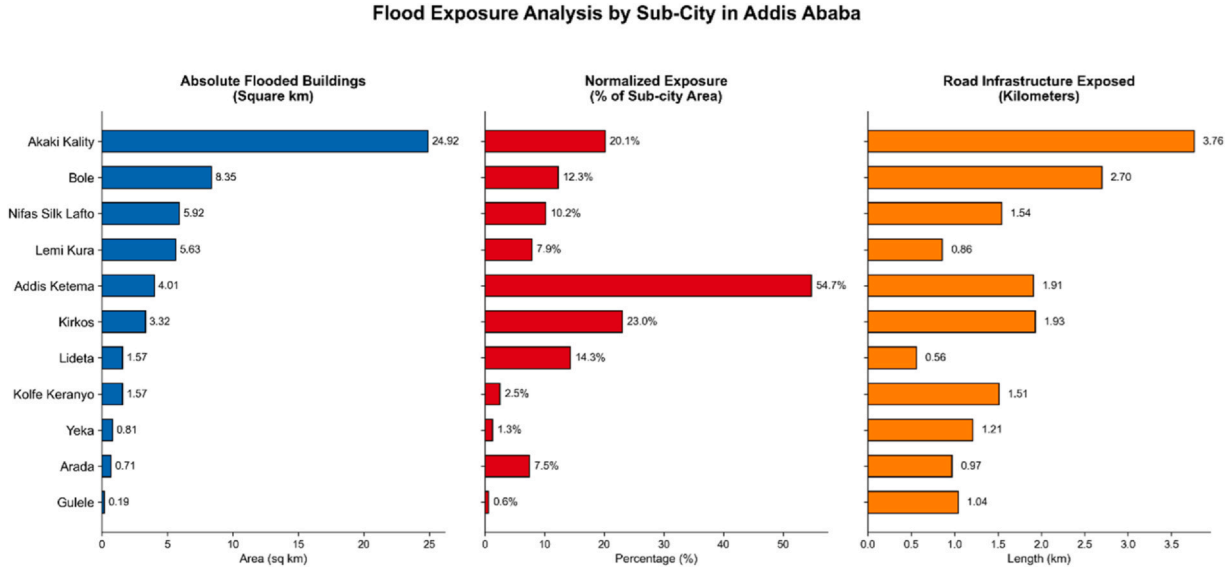


Fig. 4. Multi-dimensional flood exposure analysis across Addis Ababa sub-cities(y-axis), detailing absolute flooded building area (km^2), normalized proportional impact (% of total sub-city area), and length of exposed road infrastructure (km).

respectively. The estimated area is particularly alarming, given the areas that experienced inundation at least twice in a year were selected for analysis to identify only the high exposure hotspots.

The sub-city level analysis reveals significant spatial heterogeneity in both the scale and type of flood infrastructure exposure across Addis Ababa (Fig. 4). While Akaki Kality sustains the highest absolute damage to buildings (24.92 km^2) and roads (3.76 km),

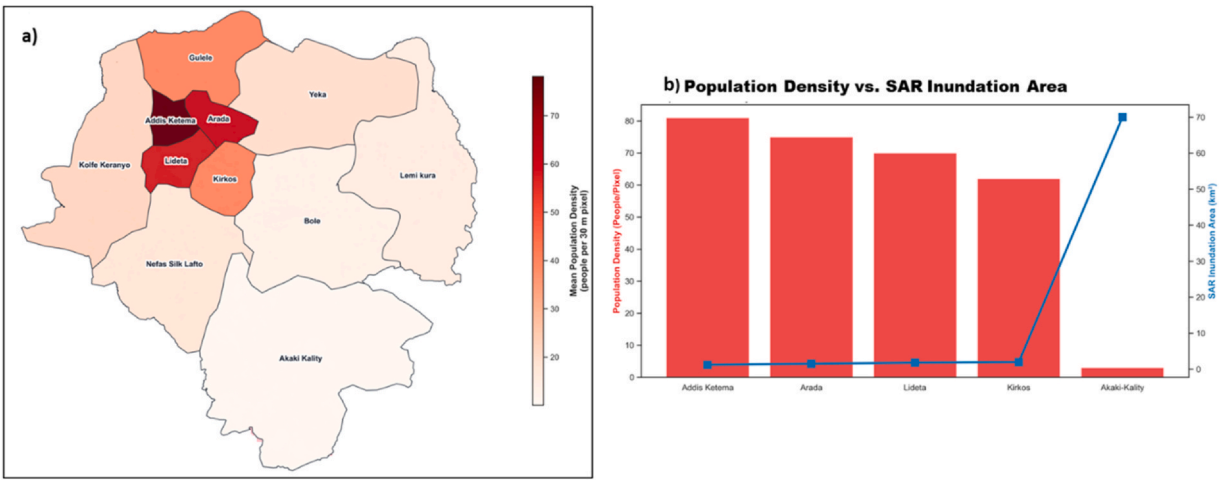


Fig. 5. Spatial distribution of population density and its relationship with SAR-derived flood inundation area across Addis Ababa sub-cities. a) mean population density (people per 30 m pixel), highlighting the densely populated urban core. b) quantification of the top five sub-cities, contrasting peak population densities (red bars) against total spatial flood extent (blue line).

normalizing the data reveals Addis Ketema as the most proportionally vulnerable, with 54.7% of its total land exposed. Furthermore, the varying ratios of building-to-road exposure across zones such as Lemi Kura's high structural damage but minimal road disruption demonstrate that raw hazard area alone is an insufficient metric for localized urban flood risk. Larger sub-cities, such as Akaki Kality, Bole, and Lemi Kura, tend to experience greater overall flood impacts, possibly due to their larger geographic size and situation in flood-prone zones. Particularly, the high exposure in Akaki Kality is largely linked to the flat terrain and extensive urbanization within the floodplain, aligning with the findings of Feyissa et al. (2018).

3.2. Population density and flood exposure

Fig. 5 illustrates the spatial distribution of population density across the sub-cities of Addis Ababa and maps this against the SAR-detected flood inundation areas. The Fig. 5a reveals a highly concentrated urban core, with sub-cities such as Addis Ketema, Lideta, and Arada exhibiting the highest mean population densities, reaching peak values of over 80 people per 30 m pixel. In contrast, peripheral sub-cities, particularly Akaki Kality in the south, exhibit vastly lower mean population densities.

An inverse relationship is observed, where highly populated sub-cities, such as Lideta, Arada, Kirkos, and Addis Ketema, experience fewer flooded pixels compared to low-density areas like Akaki-Kality as quantified in the dual-axis chart (Fig. 5b). Specifically, the high-density sub-cities have a total area of 6.45 km^2 flooded locations, whereas Akaki-Kality, a low-density sub-city, accounts for 70 km^2 of flooded locations. This trend could be attributed to the topography of low-density areas that makes them more prone to flooding; particularly Akaki-Kality is a low-lying sub-city with floodplains.

3.2.1. Comparison of SAR flood exposure map with observed flood data

The results of the comparison metrics indicate an inconsistent performance of the SAR-derived flood map when evaluated against the observed flood data. While the overall accuracy (95.8%) and F1-Score (0.984) suggest a high level of agreement between the two datasets, Cohen's Kappa (0.48) and Matthews Correlation Coefficient (0.50) reveal only moderate agreement. A key factor contributing to this inconsistency may be apparent false positives, areas where SAR indicates flooding but the observed dataset does not. However, these are likely not errors in the SAR map but rather false negatives in the observation dataset: actual flooded areas that were not captured by citizen scientists or AAFDRMC due to limited spatial coverage. If the flood observations were restricted to those obtained from the Commission (AAFDRMC), the Kappa and MCC results would likely be poorer than those currently observed. This underscores the value of citizen science data as a viable, complimentary data source (Fig. 6).

3.3. Evaluating flood exposure agreement across multiple maps

Fig. 7a presents a combined map that visually represents the spatial distribution of flood-exposed areas derived from three distinct sources: the SAR data, the hydrodynamic model, and the machine learning susceptibility map. The analysis indicates notable discrepancies in both the spatial distribution and the total quantity of flooded versus non-flooded pixels among the three methods. While a few areas show consensus across all three sources, many locations are uniquely identified by a single map, reflecting the different physical flood mechanisms each method captures.

The SAR-derived flood-exposed pixels (2404 pixels total, ≈240,400 m^2) are sparsely distributed across the study area, with concentrations predominantly in the low-lying southern end of the city. This dataset inherently captures observed pluvial (surface) flooding, pinpointing localized urban depressions where poor drainage and impermeable surfaces lead to severe waterlogging, often

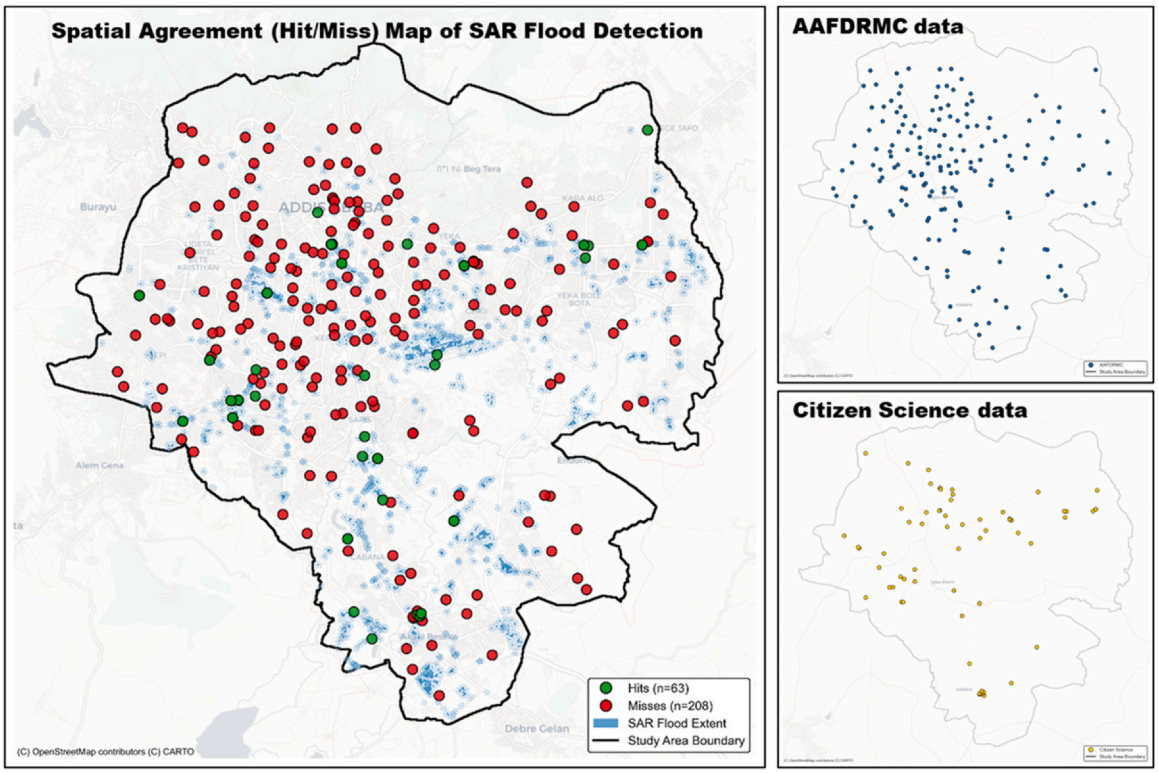


Fig. 6. Spatial validation of the SAR-derived flood map against combined observations (AAFDRMC and citizen science). True Positives (green) represent locations where the SAR model successfully detected known, flood observation locations. False Negatives (red) represent observed hotspots that the SAR map failed to detect. The overall continuous SAR flood footprint (2017–2023) is depicted in blue.

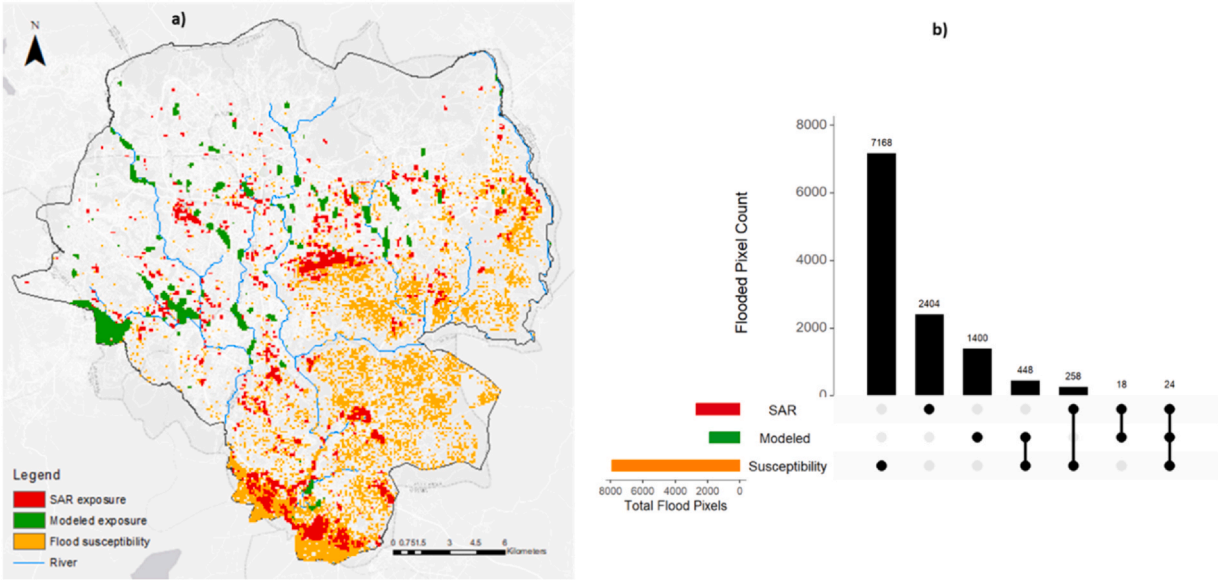


Fig. 7. a) Spatial distribution of flood exposed areas from three methods applied across the study area, Addis Ababa. Background mapping from OpenStreetMap. b) Upset plot quantifying the pixel-level spatial intersections among the three methodologies. Horizontal bars indicate the absolute total of flooded pixels identified by each individual model. Vertical bars detail the specific intersection sizes, demonstrating a high degree of unique spatial coverage (leftmost vertical bars) and a minimal multi-model consensus area where all three methodologies agree (rightmost bar, n = 24 pixels).

far from major river channels. Conversely, the modeled exposure map identifies 1400 ($\approx$140,000 m^2), flooded pixels, mostly distributed in the northern and central parts of the city. Unlike the SAR map, the hydrodynamic model's exposed pixels are closely correlated with river proximity and steep topography. Because it employs a rain-on-grid approach, it successfully captures fast-

moving fluvial runoff and flash flood routing accumulating in the high-elevation, high-slope northern catchments. Finally, the susceptibility map identifies 7168 (≈716,800 m^2) flooded pixels, which is higher than the other two methods. This indicates a much broader potential for flood exposure, particularly in the eastern-central part of the city and compounding in the southern end.

Rather than viewing these differences as mere errors, these discrepancies highlight the importance of considering methodological strengths. Urban environments like Addis Ababa experience a complex mix of riverine overtopping and localized drainage failures; thus, utilizing different mapping approaches is essential to fully capture the diverse mechanisms of urban flood hazard and exposure.

The pattern of flooded and non-flooded areas derived from individual maps was inspected using Moran's I index. A higher Moran's I value was recorded in the SAR flood exposure map (0.98) and in the flood susceptibility map (0.95); whereas, the lowest value of Moran's I was calculated as 0.25 in the modeled flood map. The higher value of Moran's I in the SAR flood exposure map and flood susceptibility map indicated a significant clustering pattern of flooded and non-flooded areas, suggesting that these areas are likely concentrated within specific geographic areas.

3.3.1. Spatial relationship between the flooded areas and topographic variables

All maps showed a strong concentration of flooded pixels in the lower elevation range (2052 - 2313 m), where more than 80% (in SAR and susceptibility maps) and 50% (modeled map) of the flooded pixels are located. In addition, 36.14% of flooded pixels are in 2314–2457 m for the modeled map. These results indicated that flooding is largely confined to lower-lying areas. The majority of flooded pixels in all three maps are concentrated in gentle slope areas (0–8.4°), which is expected as flatter terrain allows for water accumulation. The SAR-derived map has 92.6% of its flooded pixels in this range, while the modeled map has 79.8%, and the susceptibility map has a nearly identical pattern with 83.8% of flooded pixels in this range. However, the modeled map showed a slightly higher proportion of flooded pixels in moderately sloped areas (8.4–13.6°) compared to SAR and susceptibility maps. In contrast, all three maps show minimal flooding in steep slopes (above 13.6°), confirming that steeper areas in the city are less prone to flooding. The modeled flood map showed a much sharper concentration near the river, with 55.83% of flooded pixels within 626 m, indicating that the model-based approach places more emphasis on riverine flood. In contrast, the SAR-derived and susceptibility maps indicate that flooding can extend further away from the river, likely considering urban (pluvial) flooding (Table 4).

3.4. Spatial agreement assessment

The first pair, SAR and modeled exposure maps, exhibit the least spatial overlap (0.62 km^2) with a Jaccard coefficient and a Dice coefficient of 0.014 and 0.027, respectively. However, the Hausdorff distance of 2.6 km indicated the flooded pixels of this pair are located relatively close to each other. The second pair of SAR exposure map and susceptibility map, while showing slightly better agreement than the first pair with a spatial intersecting area of 4.48 km^2, still has a very low Jaccard coefficient (0.072) and Dice coefficient (0.143), reinforcing the fact that the two maps do not exhibit strong spatial alignment. The Hausdorff distance of 5.3 km in this pair further underscores these discrepancies, indicating that many flooded areas identified in the susceptibility map are spatially distant from the SAR-derived map. Lastly, the modeled and susceptibility maps exhibit 5.89 km^2 spatial extent agreement, yet their Jaccard coefficient (0.053) and Dice coefficient (0.106) still indicate poor spatial overlap. The Hausdorff distance of 8.9 km, the highest among the three comparisons, suggests their flood extents are often located far apart. The UpSet plot (Fig. 7b above) provides a direct visual quantification of the spatial (dis)agreement among the three flood exposure frameworks, mathematically reinforcing the pairwise statistical metrics (Table 5).

Table 4
Spatial relationship between the flooded area and its related topographic variable.

		No. of flooded pixels in each map					
Topographic variable	Class	**SAR derived map**	%	**Modeled map**	%	**Susceptibility map**	%
Elevation (m)	2052 - 2191	1133	47	86	6.1	2869	40.02
	2192 - 2313	972	40.5	701	50.07	3002	41.89
	2314- 2457	282	11.7	506	36.14	1267	17.67
	2458 - 2654	16	0.7	102	0.34	30	0.42
	2655 - 3027	1	0.1	5	7.30	0	0
Slope(°)	0 - 3.9	1230	51.2	675	48.21	3191	44.52
	4 - 8.4	995	41.4	443	31.64	2816	39.3
	8.5 - 13.6	149	6.17	224	16.01	990	13.84
	13.7 - 21.2	28	1.15	55	3.93	125	1.74
	21.3 - 51.9	2	0.08	3	0.21	46	0.6
Distance from river(m)	0 - 626	870	36.2	782	55.83	1781	24.84
	627 - 1438	1053	43.7	372	26.57	2785	39.85
	1439 - 2412	348	14.7	146	10.4	1967	27.43
	2413 - 3571	108	4.4	75	5.4	480	6.68
	3572 - 5914	25	1	25	1.77	155	2.2

Table 5
Spatial comparison metrics results.

Compared maps	No. of overlapping flooded pixels	Jaccard Coefficient	Dice Coefficient	Hausdorff Distance (in Kilometers)
SAR Vs. modeled	18	0.014	0.027	2.6
SAR Vs. susceptibility	258	0.072	0.143	5.3
Modeled Vs. susceptibility	448	0.053	0.106	8.9

4. Discussion

The present study systematically evaluated the spatial agreement and contextual strengths of three distinct urban flood exposure mapping methods in Addis Ababa. By developing a multi-temporal SAR-derived flood map (2017–2023), the analysis captured a comprehensive footprint of recurrent inundation events that single-pass observations often miss. This extended temporal approach is particularly valuable in a rapidly urbanizing landscape characterized by flashy, localized pluvial flooding.

Our validation strategy leveraged a synthesized dataset merging institutional records with participatory citizen science. While the citizen-science observations were collected city-wide via a network of over 260 volunteers distributed across all 11 sub-cities, the reporting was inherently opportunistic and concentrated in frequently flooded or highly accessible areas. Thus, we acknowledge this limitation that the, dataset may lack the complete, uniform spatial coverage. To partially mitigate this, we merged citizen-science points with the more systematic AAFDRMC and performed a binary confusion-matrix analysis on rasterized points. Additionally, while mobile GPS is widely adopted for data collection, it carries spatial inaccuracies in dense urban environments (typically ± 5–10 m), which we addressed through targeted field verifications. Ultimately, the validation metrics such as the high F1-score (0.984) contrasted with a moderate Kappa coefficient (0.48) reflect the spatial patchiness of these opportunistic point-based observations. Future work could strengthen validation by implementing a stratified sampling design that explicitly records both flooded and non-flooded conditions across a defined grid.

Beyond the validation of the observed SAR map, the comparative assessment of the three methodologies revealed profound spatial divergence. This was mathematically confirmed by exceptionally low Jaccard (0.014–0.072) and Dice (0.027–0.143) coefficients across all pairs. The observed spatial discrepancies highlight the fundamentally different physical phenomena and methodological assumptions captured by each approach. In this study, the SAR exposure map captured empirical records of actual, often scattered inundation footprints. This aligns with prior literature establishing that SAR's primary utility lies in retrospective and immediate damage assessment rather than predictive planning (Havivi et al., 2016). In contrast, our hydrodynamic model results predominantly delineated contiguous, scenario-based riverine flooding while systematically missing localized pluvial pooling. This behavior corroborates the established strengths of hydrodynamic models, which are generally optimized for informing targeted structural interventions along primary watercourses rather than capturing spatially diffuse events (Iliadis et al., 2023). Meanwhile, the machine learning-based susceptibility map in our analysis projected the broadest envelope of potential risk by synthesizing fixed topographic and environmental factors. As observed in similar susceptibility studies (Hitouri et al., 2024), the inherent lack of temporal specificity in this approach limits its use for event-based analysis, though our findings confirm its function as a critical baseline tool for broad, strategic vulnerability zoning. Ultimately, the minimal spatial consensus identified among the three frameworks mathematically validates that these mapping techniques do not act as redundant proxies for one another. Instead, our findings prove that relying on any single exposure map inevitably leads to a biased estimation of urban flood risk, underscoring the necessity of a multi-criteria, ensemble approach.

All three maps showed that flooding is predominantly confined to low-elevation and gentle-slope areas, yet the SAR-derived map identifies more extensive pluvial flooding farther from the river. Conversely, the flood susceptibility map exhibits a concentration of flood-prone areas in closer proximity to the river, which is expected given that distance to the river is a conditioning factor in its generation (for detail, see Asfaw et al., 2025), while the modeled flood map showed most significant flood exposure concentrated in river-adjacent areas. This difference arises because, nevertheless, recent 2D hydrodynamic models with direct rainfall inputs (such as Hec-RAS 2D used in the study of Carr et al., 2024), shown to efficiently simulate pluvial flooding, the extent to which these models produce pluvial flooding (i.e., flooding caused by intense rainfall and surface runoff that does not drain properly) depends on the model setup, input data, and parameterization.

5. Conclusion

This study provides an evaluation of urban flood exposure by integrating a multi-temporal SAR inundation map with demographic datasets, and systematically comparing it against hydrodynamic and machine-learning exposure models. The SAR-derived analysis delineated the spatial distribution of flood-affected urban systems, revealing that exposure is concentrated in low-lying peripheral sub-cities such as Akaki-Kality, despite higher population densities in the urban core. Validation against a synthesized dataset of institutional records and citizen-science observations confirmed the high overall accuracy of the SAR approach. However, it explicitly highlighted the inherent challenges of using spatially discrete, opportunistic point data to validate continuous raster maps, as unreported floods can artificially inflate false-positive error rates.

The comparative assessment demonstrated that the choice of mapping methodology fundamentally alters the resulting spatial estimation of flood exposure. The SAR map captured scattered, empirical pluvial flooding; the hydrodynamic model predominantly identified contiguous riverine exposure in the central and northern catchments; and the susceptibility model highlighted a broad

envelope of potential risk strongly tied to topographic depressions. The severe lack of spatial overlap among these models proves that they capture distinct physical flood mechanisms. Consequently, utilizing a single mapping framework risks critical miscalculations in urban flood exposure estimation.

Overall, the study presents evidence that flood extents and the consequent estimated exposure significantly vary based on the flood mapping approach adopted. The study also demonstrates that each flood mapping method needs to serve a distinct purpose. The findings emphasize that an integrated approach combining multiple mapping techniques provides critical insights for targeted emergency response, informed infrastructure planning, and proactive risk mitigation in flood-prone urban environments like Addis Ababa.

Looking forward, future validation frameworks must address the spatial biases of opportunistic reporting. Expanding and formalizing citizen science networks through structured, stratified sampling designs that explicitly require the recording of both flooded and non-flooded conditions across a defined grid will significantly strengthen model evaluation. Finally, developing an ensemble flood exposure map that synthesizes the strengths of all three methods, SAR for event-driven validation, the hydrodynamic model for scenario-based planning, and the susceptibility map for strategic zoning, and embedding this into local disaster risk management workflows represents a concrete step toward more resilient urban flood governance.

CRediT authorship contribution statement

Eden Seifu Gebre: Conceptualization, Methodology, Software, Writing – original draft. **Alemseged Tamiru Haile:** Conceptualization, Writing – review & editing. **Tilaye Worku Bekele:** Data curation, Software. **Wegayehu Asfaw:** Data curation, Software. **Mark A. Trigg:** Writing – review & editing.

References

Feyissa, G., Zeleke, G., Gebremariam, E., & Bewket, W. (2018). GIS based quantification and mapping of climate change vulnerability hotspots in Addis Ababa. *Geoenvironmental Disasters, 5*, 1–17.

Rahman, M. R., & Thakur, P. K. (2018). Detecting, mapping and analysing of flood water propagation using synthetic aperture radar (SAR) satellite data and GIS: A case study from the Kendrapara District of Orissa State of India. *The Egyptian Journal of Remote Sensing and Space Science, 21*, S37–S41.

Ramiaramanana, F. N., & Teller, J. (2021). Urbanization and floods in sub-saharan africa: Spatiotemporal study and analysis of vulnerability factors—case of antananarivo agglomeration (Madagascar). *Water, 13*(2), 149.

Al Jazeera, 2021. Deadly floods hit Ethiopia's capital Addis Ababa. Available at: ⟨https://www.aljazeera.com⟩ [Accessed 5 April 2026].

Asfaw, W., Rientjes, T., & Haile, A. T. (2023). Blending high-resolution satellite rainfall estimates over urban catchment using Bayesian Model Averaging approach. *Journal of Hydrology Regional Studies, 45*, Article 101287.

Asfaw, W., Rientjes, T.H., Bekele, T.W. and Haile, A.T., 2025. Estimating Elements Susceptible to Urban Flooding Using Multisource Data and Machine Learning. Available at SSRN 4847207.

Baddianaah, I. (2023). We all share the blame: Analyzing the root causes of flooding in African cities with specific reference to Harper City, Liberia. *Environmental Challenges, 13*, Article 100790.

Bekele, T. W., Haile, A. T., Trigg, M. A., & Walsh, C. L. (2022). Evaluating a new method of remote sensing for flood mapping in the urban and peri-urban areas: Applied to Addis Ababa and the Akaki catchment in Ethiopia. *Natural Hazards Research, 2*(2), 97–110.

Bentivoglio, R., Isufi, E., Jonkman, S. N., & Taormina, R. (2022). Deep learning methods for flood mapping: A review of existing applications and future research directions. *Hydrology and Earth System Sciences Discussions, 2022*, 1–50.

Birhanu, D., Kim, H., Jang, C., & Park, S. (2016). Flood risk and vulnerability of Addis Ababa City due to climate change and urbanization. *Procedia Engineering, 154*, 696–702.

Carr, A. B., Trigg, M. A., Haile, A. T., Bernhofen, M. V., Alemu, A. N., Bekele, T. W., & Walsh, C. L. (2024). Using global datasets to estimate flood exposure at the city scale: An evaluation in Addis Ababa. *Frontiers in Environmental Science, 12*, Article 1330295.

Cohen, J. (1960). A Coefficient of Agreement for Nominal Scales. *Educational and Psychological Measurement, 20*(1), 37–46.

CRED (Centre for Research on the Epidemiology of Disasters), 2022. Natural Disasters 2022. Brussels: CRED. Available at: ⟨https://www.emdat.be⟩ [Accessed 25 April 2025].

De Brito, M. M., & Evers, M. (2016). Multi-criteria decision-making for flood risk management: A survey of the current state of the art. *Natural Hazards and Earth System Sciences, 16*(4), 1019–1033.

De Moel, H. D., van Alphen, E. J., & Aerts, J. C. (2009). Flood maps in Europe–methods, availability and use. *Natural hazards and earth System Sciences, 9*(2), 289–301.

Esri, 2023. *Esri 10-Meter Land Cover*. Redlands, CA: Environmental Systems Research Institute (Esri), Impact Observatory, and Microsoft. Available at: ⟨https://livingatlas.arcgis.com/landcover/⟩ [Accessed 6 April 2026].

Ethiopian Meteorology Institute (EMI), 2023. Annual Climate Bulletin for the year 2023. Addis Ababa, Ethiopia: EMI.

CSA). (2013). Population Projections for Ethiopia (2007–2037). Addis Ababa: CSA. Available at: ECDE Knowledge Hub [Accessed 25 January 2025].

Feizbahr, M., Brake, N., Arbabkhah, H., Asli, H. H., & Woods, K. (2025). Flood Susceptibility Mapping Using Machine Learning and Geospatial-Sentinel-1 SAR Integration for Enhanced Early Warning Systems. *Remote Sensing, 17*(20), 3471.

FloodList, 2021. Ethiopia – Deadly Floods in Addis Ababa. Available at: ⟨http://floodlist.com⟩ [Accessed 6 April 2026].

Havivi, S., Schvartzman, I., Maman, S., Marinoni, A., Gamba, P., Rotman, S.R., & Blumberg, D.G., 2016. Utilizing SAR and Multispectral Integrated Data for Emergency Response. ISPRS Archives, XLI-B7, pp. 493–500.

Herfort, B., Lautenbach, S., Porto de Albuquerque, J., Anderson, J., & Zipf, A. (2023). A spatio-temporal analysis investigating completeness and inequalities of global urban building data in OpenStreetMap. *Nature Communications, 14*(1), 3985.

Hitouri, S., Mohajane, M., Lahsaini, M., Ali, S. A., Setargie, T. A., Tripathi, G., D'Antonio, P., Singh, S. K., & Varasano, A. (2024). Flood susceptibility mapping using SAR data and machine learning algorithms in a small watershed in northwestern Morocco. *Remote Sensing, 16*(5), 858.

Iliadis, C., Galiatsatou, P., Glenis, V., Prinos, P., & Kilsby, C. (2023). Urban flood modelling under extreme rainfall conditions for building-level flood exposure analysis. *Hydrology, 10*(8), 172.

Jalayer, F., De Risi, R., De Paola, F., Giugni, M., Manfredi, G., Gasparini, P., Topa, M. E., Yonas, N., Yeshitela, K., Nebebe, A., & Cavan, G. (2014). Probabilistic GIS-based method for delineation of urban flooding risk hotspots. *Natural hazards, 73*, 975–1001.

Landis, J. R., & Koch, G. G. (1977). The measurement of observer agreement for categorical data. *Biometrics, 33*(1), 159–174.

Lin, L., Di, L., Yu, E. G., Kang, L., Shrestha, R., Rahman, M. S., Tang, J., Deng, M., Sun, Z., Zhang, C., & Hu, L. (2016). *A review of remote sensing in flood assessment* (July) *2016 Fifth International Conference on Agro-Geoinformatics (Agro-Geoinformatics)*. IEEE,1–4 (July).

Matthews, B. W. (1975). Comparison of the predicted and observed secondary structure of T4 phage lysozyme. *Biochimica et Biophysica Acta (BBA)-Protein Structure, 405*(2), 442–451.

Moges, S. A., Taye, M. T., Willems, P., & Gebremichael, M. (2014). Exceptional pattern of extreme rainfall variability at urban centre of Addis Ababa, Ethiopia. *Urban Water Journal, 11*(7), 596–604.

Moisa, M. B., Merga, B. B., & Gemeda, D. O. (2022). Flood susceptibility mapping by integrating GIS-based multi-criteria decision analysis and analytical hierarchy process in the Wabi Shebele River Sub-basin, Ethiopia. *Journal of Flood Risk Management*.

Moran, P. A. P. (1950). Notes on continuous stochastic phenomena. *Biometrika, 37*(1/2), 17–23.

Papilloud, T., Steiner, A., Zischg, A.P., and Keiler, M., 2019. Road Network Disruptions During Extreme Flooding Events and Their Impact on the Access to Emergency Medical Services: A Spatiotemporal Vulnerability Analysis. SSRN.

ReliefWeb, 2023. Ethiopia: Flood Snapshot (May 2023). Available at: ⟨https://reliefweb.int⟩ [Accessed 25 April 2025].

Sejinja, N. et al., 2025. (Please verify the exact title for Sejinja in your library, likely a forthcoming paper).

Tiepolo, M., Abraiz, M., Ibrahim, M. H., Baoua, O., Cannella, G., Gutierrez, A. M., & Saretto, F. (2025). Flood risk assessment along the River Niger. *Mendeley Data, V3*.

Tran, H. N., Rutten, M., Prajapati, R., Tran, H. T., Duwal, S., Nguyen, D. T., Davids, J. C., & Miegel, K. (2024). Citizen scientists' engagement in flood risk-related data collection: a case study in Bui River Basin, Vietnam. *Environmental Monitoring and Assessment, 196*(3), 280.

UN OCHA). (2024). *Eastern Africa: Humanitarian Snapshot (December 2024)*. Geneva: UN OCHA. Available at: UN OCHA [Accessed 25 April 2025].

Ziegelaar, M., & Kuleshov, Y. (2022). Flood exposure assessment and mapping: A case study for Australia's Hawkesbury-Nepean catchment. *Hydrology, 9*(11), 193.